



PCCP

Proton Affinities of Pertechnetate (TcO₄⁻) and Perrhenate (ReO₄⁻)

| | |
|-------------------------------|---|
| Journal: | <i>Physical Chemistry Chemical Physics</i> |
| Manuscript ID | CP-ART-03-2020-001721.R1 |
| Article Type: | Paper |
| Date Submitted by the Author: | 12-May-2020 |
| Complete List of Authors: | Jian, Jiwen; Hangzhou Institute of Advanced Studies, Varathan, E.; University of Manitoba, Department of Chemistry Cheisson, Thibault; University of Pennsylvania, Chemistry Jian, Tian; E O Lawrence Berkeley National Laboratory, Chemical Sciences Lukens, Wayne; Lawrence Berkeley National Laboratory, c Chemical Sciences Division Davis, Rebecca; University of Manitoba, Chemistry Schelter, Eric J; University of Pennsylvania, Department of Chemistry Schreckenbach, Georg; University of Manitoba, Department of Chemistry Gibson, John; Lawrence Berkeley National Laboratory, Chemical Sciences Division |
| | |

SCHOLARONE™
Manuscripts

Proton Affinities of Pertechnetate (TcO_4^-) and Perrhenate (ReO_4^-)

Jiwen Jian^{1,a}, Elumalai Varathan², Thibault Cheisson^{3,b}, Tian Jian¹, Wayne W. Lukens¹,
Rebecca L. Davis², Eric J. Schelter³, Georg Schreckenbach^{2*}, John K. Gibson^{1,*}

¹Chemical Sciences Division, Lawrence Berkeley National Laboratory, Berkeley, California, 94720, USA

²Department of Chemistry, University of Manitoba, Winnipeg, Manitoba, R3T 2N2, Canada

³Department of Chemistry, University of Pennsylvania, Philadelphia, Pennsylvania, 19104, USA

*Corresponding authors: schrecke@cc.umanitoba.ca; jkgibson@lbl.gov

^aPresent address: Hangzhou Institute of Advanced Studies, Zhejiang Normal University, 1108 Gengwen Road, Hangzhou, Zhejiang, 311231, China.

^bPresent address: Eramet Ideas. 1 avenue Albert Einstein, 78190 Trappes, France.

Abstract

The anions pertechnetate, TcO_4^- , and perrhenate, ReO_4^- , exhibit very similar chemical and physical properties. Revealing and understanding disparities between them enhances fundamental understanding of both. Electrospray ionization generated the gas-phase proton bound dimer $(\text{TcO}_4^-)(\text{H}^+)(\text{ReO}_4^-)$. Collision induced dissociation of the dimer yielded predominantly HTcO_4 and ReO_4^- , which according to Cooks' kinetic method indicates that the proton affinity (PA) of TcO_4^- is greater than that of ReO_4^- . Density functional theory computations agree with the experimental observation, providing $\text{PA}[\text{TcO}_4^-] = 300.1$ kcal/mol and $\text{PA}[\text{ReO}_4^-] = 297.2$ kcal/mol. Attempts to rationalize these relative PAs based on elementary molecular parameters such as atomic charges indicate that the entirety of bond formation and concomitant bond disruption needs to be considered to understand the energies associated with such protonation processes. Although in both the gas and solution phases, TcO_4^- is a stronger base than ReO_4^- , it is noted that the significance of even such qualitative accordance is tempered by the very different natures of the underlying phenomena.

Introduction

Pertechnetate, TcO_4^- , and perrhenate, ReO_4^- , are tetrahedral anions that exhibit very similar chemistry. With the negative charge distributed among four oxygen atoms, these MO_4^- ions, like ClO_4^- ,¹ exhibit “soft” coordination behavior that results in outer sphere complexation in solution and relatively modest hydration energies.² Extensive efforts aimed at selective removal of TcO_4^- from aqueous solution reflects the fact that it is the predominant and environmentally mobile form of radioactive ^{99}Tc , which is a prevalent and problematic nuclear fission product.³ Separation of ReO_4^- from other anions has received less attention than TcO_4^- , but is nonetheless of interest given potential applications of beta-emitting ^{188}Re (16.9 h half-life) in nuclear medicine.⁴ Pursuit of selective receptors for TcO_4^- and ReO_4^- generally has an ultimate goal of separation from other environmentally and industrially prevalent anions such as Cl^- , NO_3^- and SO_4^{2-} .⁵⁻⁷ Less familiar, and generally less imperative from a practical perspective, is the much more challenging separation of TcO_4^- and ReO_4^- from one another. Successful separation of these two chemically similar species would advance their separations from other anions. In addition, widespread use of ReO_4^- containing stable naturally occurring isotopes of Re as a surrogate for radioactive $^{99}\text{TcO}_4^-$ motivates understanding differences between these two species.⁸ Furthermore, as for other chemically similar elements in the same group of the periodic table, revealing fundamental differences between Tc and Re is key to better comprehending the chemistry of both.

The original objective of this work was to assess comparative affinities of TcO_4^- and ReO_4^- for an organic ligand that can readily form hydrogen bonds, namely the protonated tripodal nitroxide ligand $[(2\text{-}^t\text{BuNOH})\text{C}_6\text{H}_4\text{CH}_2]_3\text{N}$, denoted as H_3TriNOx and shown in Figure 1.⁹ H_3TriNOx presents three accessible hydroxyl moieties as potential H-bonding sites.¹⁰ The strategy was to use electrospray ionization (ESI) to generate gas-phase complexes comprising TcO_4^- and/or ReO_4^- coordinated by H_3TriNOx . It was anticipated that relative abundances of different complexes would reveal differences in efficacy of anion coordination by the ligand, and that collision induced dissociation (CID) might reveal differences in anion-ligand binding. The gas-phase results indeed suggested a preference for association of H_3TriNOx with TcO_4^- over ReO_4^- .

Perrhenic acid, HReO_4 , was first reported ~90 years ago,¹¹ pertechnic acid, HTcO_4 , ~70 years ago,¹² and comparison of properties of the two was reported ~60 years ago.¹³ For the current work, ESI studies revealed the gas-phase, bimetallic dimer of the two conjugate bases linked by a proton, $(\text{TcO}_4^-)(\text{H}^+)(\text{ReO}_4^-)$, which is a more fundamentally interesting and pertinent species than the initially pursued H_3TriNOx -containing complexes noted above. In the simple dimer, the two tetroxide anions are bound by a proton, with a net charge of -1 on the complex. This proton-bound dimer presented the opportunity to evaluate the relative proton affinities (PAs) of TcO_4^- and ReO_4^- using Cooks’ kinetic method.¹⁴⁻¹⁶ In addition to their proton bridge, some proton-bound dimers can exhibit secondary bonding interactions between the constituent anions, which can complicate interpretations in the context of relative PAs.¹⁷ Accordingly, an important attribute of $(\text{TcO}_4^-)(\text{H}^+)(\text{ReO}_4^-)$ is that the structure and resulting bonding interaction can confidently be assigned as simple proton-bound dimer $[\text{O}_3\text{Tc}-\text{O}\cdots\text{H}\cdots\text{O}-\text{ReO}_3]^-$, such that its CID should indicate the relative PAs of TcO_4^- and ReO_4^- . Reported here is the result, based on CID of $(\text{TcO}_4^-)(\text{H}^+)(\text{ReO}_4^-)$, that the

PA[TcO₄⁻] is greater than the PA[ReO₄⁻]. Density functional theory (DFT) computations performed to understand this conclusion provided the anticipated relationship—PA[TcO₄⁻] > PA[ReO₄⁻—and showed that the difference is small, as expected for two such similar anions. Attempts to rationalize the relationship between these two PAs based on elementary molecular parameters suggest intertwined effects upon protonation that cannot be clearly resolved. Comparison of the gas-phase molecular properties with related solution properties such as basicities of TcO₄⁻ versus ReO₄⁻ reveals apparent correlations, but also provides caution against overreach of the significance of such correlations.

Experimental Methods

Caution – The ⁹⁹Tc used in this work is radioactive and must be handled only with appropriate precautions in a suitable radiological laboratory.

Gas phase experiments were performed using an Agilent 6340 quadrupole ion trap mass spectrometer (QIT/MS) with an ESI source inside a radiological containment glovebox.¹⁸ H₃TriNO_x was synthesized as reported previously.⁹ Anion complexes were produced by ESI of a solution containing ~100 μM of H₃TriNO_x and ~500 μM of both NH₄⁹⁹TcO₄ and NH₄ReO₄ (isotopically natural Re) in ethanol (<10% water). Ions with a specific mass-to-charge ratio (m/z) are isolated and subjected to CID whereby they are resonantly excited and undergo energetic collisions with He, which ultimately leads to ion dissociation. CID products are identified by mass selective ion ejection from the QIT to a detector. Negative ion mass spectra were acquired using the following instrumental parameters: solution flow rate = 60 μL min⁻¹; nebulizer gas pressure = 15 psi; capillary voltage = +3500 V; end plate voltage offset = -500 V; dry gas flow rate = 5 L/min; dry gas temperature = 325 °C; capillary exit = -136.0 V; skimmer = -40.0 V; octopole 1 and 2 dc = -12.0 and -1.74 V; octopole RF amplitude = 200.0 Vpp; lens 1 and 2 = 5.0 and 60 V; trap drive = 74. Gas for ESI nebulization and drying in the ion transfer capillary was the boil off from liquid nitrogen. Results were obtained using nominal CID energies of ~0.2-0.6 V, with the specific value depending on ease of ion fragmentation. The CID voltage is an instrumental parameter that provides an indication of relative ion excitation, not actual ion energies.

Computational Methods

Scalar relativistic Density Functional Theory (DFT) calculations were performed with the Gaussian 09¹⁹ and ADF^{20,21} software packages for the geometry optimizations and vibrational frequency analyses. The ground state geometries of all molecules were fully optimized in the gas phase without any symmetry constraints. Vibrational frequency analysis assured that the optimized structures are real minima on the potential energy surface. The calculated vibrational frequencies were obtained using the harmonic approximation. For the Gaussian calculations, scalar relativistic Stuttgart energy-consistent relativistic pseudopotentials and the associated ECP60MWB_ANO valence basis sets (SDD)²² were used for the transition metal atoms. The split-valence double- ζ basis sets with polarization functions and diffusion functions on both heavy and hydrogen atoms (6-31++G**) ^{23,21} of Pople et al. were used for the remaining atoms (H, C, N and O). All

calculations employed the B3LYP^{24,25} hybrid functional, owing to its overall good performance for computing geometries of transition metal complexes. The basis set dependence of the energetics was studied with the 6-31G*, 6-311+G* and 6-31++G** basis sets, along with the same B3LYP functional. The natural atomic charges and bond orders were obtained by natural bond orbital (NBO) analysis utilizing the NBO6.0 code.^{26,27}

To further understand the influence of relativistic effects on the gas-phase reaction energetics, geometry optimizations were performed with two different functionals (B3LYP and B3LYP-D3)²⁸ with the ADF code.²⁰ The scalar zeroth-order regular approximation (ZORA)²⁹ was used to model relativistic effects, in conjunction with Slater type orbitals (STOs) of TZP quality (triple-zeta plus polarization functions).³⁰ Non-relativistic calculations were performed with similar basis sets. Geometry optimizations were performed without any symmetry constraints. Optimized geometries were always verified as minima on the potential energy surface by calculating the harmonic vibrational frequencies at the stationary point. The default convergence criterion of 10^{-6} au and an integration parameter of 6.0 were applied.

Results and Discussion

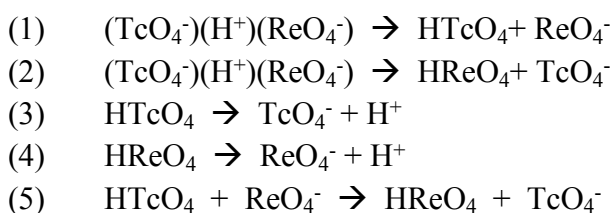
Electrospray Ionization and Collision Induced Dissociation

An ESI mass spectrum for a solution containing $H_3\text{TriNO}_x$ (denoted as L), TcO_4^- and ReO_4^- is shown in Figure 2. Dominant species are complexes $(L)[(\text{TcO}_4^-)(\text{H}^+)(\text{TcO}_4^-)]$, $(L)[(\text{TcO}_4^-)(\text{H}^+)(\text{ReO}_4^-)]$ and $(L)[(\text{ReO}_4^-)(\text{H}^+)(\text{ReO}_4^-)]$, where the indicated constituent moieties, $H_3\text{TriNO}_x$ (L) and proton-bridged permetallate dimers, are based on results given below. Bare TcO_4^- and ReO_4^- are also significant ions in the ESI mass spectrum. Minor or negligible species include $(L)(\text{TcO}_4^-)$, $(L)(\text{ReO}_4^-)$, $(\text{TcO}_4^-)(\text{H}^+)(\text{TcO}_4^-)$, $(\text{TcO}_4^-)(\text{H}^+)(\text{ReO}_4^-)$ and $(\text{ReO}_4^-)(\text{H}^+)(\text{ReO}_4^-)$. There are apparently thermodynamic and/or kinetic factors that stabilize the three dominant larger coordination complex permetallate dimers relative to these smaller constituents, at least in gas phase. The ion abundances in the mass spectrum in Figure 2 suggest preferential formation of gas-phase complexes comprising TcO_4^- over ReO_4^- . Considering that ReO_4^- abundances are distributed between two naturally occurring isotopes, ^{185}Re (37.4%) and ^{187}Re (62.6%), the net relative abundances of the complexes are: 1.00 $(L)[(\text{TcO}_4^-)(\text{H}^+)(\text{TcO}_4^-)]$: 0.90 $(L)[(\text{TcO}_4^-)(\text{H}^+)(\text{ReO}_4^-)]$; and 0.23 $(L)[(\text{ReO}_4^-)(\text{H}^+)(\text{ReO}_4^-)]$. The somewhat lower yield of the last of these suggests favored incorporation of TcO_4^- over ReO_4^- . It should be emphasized that this selectivity may not reflect solution speciation, but rather kinetic and/or energetic effects of ESI, which is a complex “solution-to-gas” process. Nevertheless, this apparent gas-phase separation factor is significantly greater than typically obtained for separating TcO_4^- from ReO_4^- in solution.³¹ It should also be noted that a separation factor in solution of 1.00:0.23 at 300 K would correspond to a difference in complexation free energies of only ~ 0.9 kcal/mol (i.e., $\Delta G = -RT\ln K$).

To further probe the structure of $(L)[(\text{TcO}_4^-)(\text{H}^+)(\text{ReO}_4^-)]$ and the possibility of preferential binding of TcO_4^- over ReO_4^- , the complex was isolated and subjected to CID, with results shown in Figure 3. The employed CID energy of only 0.20 V is qualitatively rather low when compared, for example, with 0.55 V required to fragment protonated $H_4\text{TriNO}_x^+$ (HL^+ , Figure S1). The

dominant CID process apparent in Figure 3 is neutral H_3TriNOx ligand loss to yield $(\text{TcO}_4^-)(\text{H}^+)(\text{ReO}_4^-)$. This principal pathway suggests a structure characterized by a H_3TriNOx ligand weakly bound to the bimetallic dimer, as we imply by the nomenclature $(\text{L})[(\text{TcO}_4^-)(\text{H}^+)(\text{ReO}_4^-)]$. Also apparent in Figure 3 is a small peak corresponding to ReO_4^- , which is also observed upon CID of $(\text{TcO}_4^-)(\text{H}^+)(\text{ReO}_4^-)$, as discussed below.

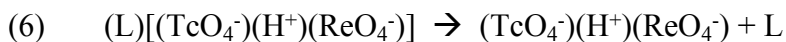
The appearance of the proton-bound dimer $(\text{TcO}_4^-)(\text{H}^+)(\text{ReO}_4^-)$ presented the opportunity to probe the relative PAs of TcO_4^- and ReO_4^- using Cooks' kinetic method.¹⁴ For two generic bases B1 and B2 bound by a proton in dimer $(\text{B1})(\text{H}^+)(\text{B2})$, this simple approach reveals the base with the higher PA is that which preferentially retains the proton upon CID. The yield of dimer $(\text{TcO}_4^-)(\text{H}^+)(\text{ReO}_4^-)$ produced by CID of $(\text{L})[(\text{TcO}_4^-)(\text{H}^+)(\text{ReO}_4^-)]$ was insufficient for secondary CID. Instead, the protonated bimetallic dimer was isolated from the parent ESI mass spectrum (Figures 2 and S2), with results for its CID shown in Figure 4. The two CID pathways for evaluating relative PAs of TcO_4^- and ReO_4^- are given by reactions (1) and (2). It is apparent from Figure 4 that reaction (1) is dominant, with only minor ($\sim 1\%$) contribution from reaction (2). The CID energy used to fragment $(\text{TcO}_4^-)(\text{H}^+)(\text{ReO}_4^-)$, 0.25 V, is only slightly higher than the 0.20 V to eliminate a ligand from $(\text{L})[(\text{TcO}_4^-)(\text{H}^+)(\text{ReO}_4^-)]$ (Figure 3). The result that reaction (1) dominates over reaction (2) indicates that $\text{PA}[\text{TcO}_4^-] > \text{PA}[\text{ReO}_4^-]$, where these PAs are defined as the enthalpies for dissociation reactions (3) and (4). Proton transfer reaction (5) is merely the difference between reactions (2) and (1), and also the difference between reactions (4) and (3). Some pertinent thermodynamics for these reactions are summarized by the following relationships: $\Delta\text{H}_3 \equiv \text{PA}[\text{TcO}_4^-]$; $\Delta\text{H}_4 \equiv \text{PA}[\text{ReO}_4^-]$; $\Delta\text{H}_5 = \Delta\text{H}_2 - \Delta\text{H}_1 = \text{PA}[\text{TcO}_4^-] - \text{PA}[\text{ReO}_4^-]$. The result that CID of $[(\text{TcO}_4^-)(\text{H}^+)(\text{ReO}_4^-)]$ yields ReO_4^- via reaction (1) indicates that $\Delta\text{H}_2 > \Delta\text{H}_1$, $\Delta\text{H}_5 > 0$, and $\text{PA}[\text{TcO}_4^-] > \text{PA}[\text{ReO}_4^-]$.



Computed Structures and Energies of Complexes

To understand the experimental observations, structures and energies of selected complexes were computed. The computed lowest energy structure of $(\text{L})[(\text{TcO}_4^-)(\text{H}^+)(\text{ReO}_4^-)]$ is shown in Figure 5, with other low-energy structures shown in SI. The structure is characterized by two hydrogen bonds between hydroxyl groups of the ligand and the metal oxo moieties. Computed energies for selected dissociations of $(\text{L})[(\text{TcO}_4^-)(\text{H}^+)(\text{ReO}_4^-)]$ are summarized in Table 1. In accord with the CID results in Figure 3, the lowest energy pathway is the observed ligand elimination reaction (6). Also apparent in the CID mass spectrum in Figure 3 is a smaller peak assigned as ReO_4^- , which can be attributed to secondary dissociation via reaction (1) that was dominant for CID of $(\text{TcO}_4^-)(\text{H}^+)(\text{ReO}_4^-)$. The structures here contrast with those previously

reported for analogous species comprised of H_3TriNOx and halide anions.¹⁰ The complex $[\text{L}(\text{HClBr})]^-$, for example, is not a $(\text{Cl}^-)(\text{H}^+)(\text{Br}^-)$ proton bound dimer coordinated by H_3TriNOx . Instead, it is essentially a protonated $\text{H}_4\text{TriNOx}^+$ coordinated by well-separated halide anions, Cl^- and Br^- . As a result, CID of $[\text{L}(\text{HClBr})]^-$ does not result in neutral H_3TriNOx ligand elimination in analogy to reaction (6), but rather HCl elimination to yield $[\text{L}(\text{Br})]^-$. The different structures and behavior reflect that, in contrast to the bulky permetallate tetroxide anions, compact halide anions can form multiple hydrogen bonds to H_3TriNOx .



The energy computed for reaction (6) using the 6-31G* basis set is substantially negative, $\Delta E_6 = -16.84$ kcal/mol. This result suggests a net repulsive interaction between H_3TriNOx and $(\text{TcO}_4^-)(\text{H}^+)(\text{ReO}_4^-)$, which would be remarkable given the hydrogen bonds—which are likely weak but presumably not repulsive—that are apparent in the structure shown in Figure 5. However, the energy for reaction (6) using instead the 6-311+G* basis set is only very slightly negative, $\Delta E_6 = -0.17$ kcal/mol. The 16.7 kcal/mol difference in the computed energy for reaction (6) using these two basis sets indicates substantial uncertainties in the energies in Table 1. Despite these uncertainties, the results in Table 1 show that the observed CID pathway is the lowest in energy, and the ligand is only weakly bound in $(\text{L})[(\text{TcO}_4^-)(\text{H}^+)(\text{ReO}_4^-)]$. Given that quantifying ligand dissociation according to reaction (6) was not of primary interest, additional computations were not pursued to further refine the energy for this process.

The principal focus was instead on the simple observed CID process given by reaction (1), which dominated over alternative reaction (2). The computed energies for reactions (1) and (2) are summarized in Table 2, with the B3LYP/SDD/6-31++G** optimized structures of the involved species shown in Figure 6. The computed structure of ReO_4^- is very similar to that previously reported by Wang and coworkers,³² with the Re-O distance found here being only 0.01 Å longer. The rather low energies for reactions (1) and (2), ~30 kcal/mol, are consistent with the low CID voltage needed to drive the reaction. In contrast to the 16.6 kcal/mol change in the energy for reaction (5) upon switching from basis set 6-31G* to 6-311+G*, the variations in computed energies for reactions (1) and (2) were much smaller for all the Gaussian basis sets employed (6-31G*, 6-311+G* and 6-31++G**). To further understand the influence of relativistic effects on the gas-phase reaction energetics of reactions (1) and (2), frozen core scalar ZORA calculations have been performed with two different functionals (B3LYP and B3LYP-D3) with the ADF code (ZORA-TZP basis sets). The resulting energies in Table 2 reveal that reaction (1) is thermodynamically favored over reaction (2), which is consistent with the Gaussian ECP results. Most significantly, the computations indicate that reaction (1) is lower in energy than reaction (2), by ~3 kcal/mol at all the considered levels of theory. The computations thus concur with the observation that CID reaction (1) is dominant, and the resulting interpretation that $\text{PA}[\text{TcO}_4^-] > \text{PA}[\text{ReO}_4^-]$. The absolute PAs computed using B3LYP/SDD/6-31++G** are $\text{PA}[\text{TcO}_4^-] = 300.07$ kcal/mol and $\text{PA}[\text{ReO}_4^-] = 297.23$ kcal/mol, which yield a difference of 2.84 kcal/mol that

corresponds to ΔH_5 in Table 2. To assess different functionals, PAs were computed at the ZORA/TZP level with DFT functionals B3LYP, B3LYP-D3, PBE0, PBE, M06-2X, and CAM-B3LYP (SI Table S4). For each functional PA[TcO₄⁻] is greater than PA[ReO₄⁻], with the difference ranging from 2.96 kcal/mol for PBE to 4.55 kcal/mol for CAM-B3LYP. Similarly, using basis sets B3LYP/TZP and B3LYP/TZ2P the calculated PA[TcO₄⁻] is greater than PA[ReO₄⁻], by 3.13 kcal/mol and 2.82 kcal/mol, respectively (SI Table S5). Although the disparity between the PAs is small—ca. 1% of their absolute values of ~300 kcal/mol—the slightly higher PA[TcO₄⁻] is clearly manifested in CID (Figure 4).

Assessment of Bonding and Proton Affinities of TcO₄⁻ and ReO₄⁻

To understand the origins of the relative PAs of TcO₄⁻ and ReO₄⁻ we consider the structures and bond parameters for the species shown in Figure 6. Some pertinent parameters are shown in Figure 6 and Table 3, with additional values in Supporting Information. The NPA charges indicate significantly more negative charges on the O atoms in ReO₄⁻ ($\delta = -0.67$) versus TcO₄⁻ ($\delta = -0.57$), a result in accord with previous computational assessments.^{31,33} A resulting straightforward prediction from more negative charges on the O atoms of ReO₄⁻ versus TcO₄⁻ is that PA[ReO₄⁻] should be greater than PA[TcO₄⁻], which contrasts with the experimental and computational results.

A complete assessment must consider charges on all O atoms before and after protonation. The charge on the protonated O is -0.84 in HReO₄ and -0.78 in HTcO₄, suggesting again that PA[ReO₄⁻] should be greater than PA[TcO₄⁻]. The charges on the other three O atoms are also more negative for HReO₄ (-0.50) versus HTcO₄ (-0.37). Upon protonation, for both the Re and Tc species the charge on the added H is ~0.53, the total charge on the four O atoms becomes less negative by 0.37, and the charge on the metal center becomes more positive by 0.10. Despite these similarities, a notable difference between the two systems is a slightly different charge redistribution upon protonation, with a result that the charge on the protonated O becomes more negative by -0.17 for HReO₄, while by -0.21 for HTcO₄. This polarization difference is insufficient to render the O charge more negative in the latter, such that there remains an apparent inconsistency between the relative PAs and O atom charges.

A key underlying consideration for understanding the apparent inconsistency between O atom charges and PA is that PA, like any reaction energy, is a function of all changes in bonding between reactants and products. Thus, PA not only reflects the attractive interaction between H⁺ and the O^{- δ} in metal oxo MO₄⁻; it also reflects changes in charges and bonds in the MO₄⁻ moiety that result from perturbations introduced by proton association. The NPA charges in Figure 6 indicate that the bonds in both ReO₄⁻ and HReO₄ are significantly more polar—i.e. more ionic and less covalent—than the corresponding bonds in TcO₄⁻ and HTcO₄. Although the bonding is not quantified here, it is reasonable that the changes in charge distribution due to protonation should more substantially disrupt the more ionic bonds in ReO₄⁻ versus those in more covalent TcO₄⁻. Such disruption that results in bond weakening should disfavor protonation and diminish the relative PA of ReO₄⁻. It should be emphasized that the difference between PA[TcO₄⁻] and

PA[ReO₄⁻] is minor relative to the overall metal-oxo bonding that is perturbed upon protonation. A key point is that relative PAs of inorganic species like these cannot necessarily be predicted from elementary molecular parameters such as effective atomic charges; the holism of perturbations needs to be considered.

From the parameters in Figure 6 for (TcO₄⁻)(H⁺)(ReO₄⁻) it is evident that the higher PA for TcO₄⁻ versus ReO₄⁻ is clearly revealed in the structure of the protonated dimer. In accord with ultimate dissociation to HTcO₄ and ReO₄⁻, the O₃TcO-H distance (1.12 Å) in the dimer is significantly shorter than the O₃ReO-H distance (1.29 Å). In lieu of the simplified representation as (TcO₄⁻)(H⁺)(ReO₄⁻), the following actual computed charges on the three moieties in the complex are obtained from the constituent atomic charges (Table S2): (TcO₄^{-0.715})(H^{+0.533})(ReO₄^{-0.815}). Although such charge assignments are not physically observable quantities, they do indicate relative charge distributions. In view of the less negative O atom charges in bare TcO₄⁻ versus ReO₄⁻, it is tempting to attribute the greater PA[TcO₄⁻] versus PA[ReO₄⁻] to the greater polarizability of Tc (79 au) and TcO₄⁻ (computed here as 57.3 au) relative to Re (62 au) and ReO₄⁻ (computed as 56.3 au).³⁴ However, as noted above, after proton association the charge on O^δ in the hydroxyl group in HTcO₄ (δ = 0.78) remains less negative than that in HReO₄ (δ = 0.84). In accord with the higher polarizability of TcO₄⁻, the enhancement in negative charge on the protonated O atom is greater for the conversion of TcO₄⁻-to-HTcO₄ (Δδ = 0.21) than for ReO₄⁻-to-HReO₄ (Δδ = 0.17). However, the difference in polarization upon protonation is insufficient to yield a more negative oxygen charge in HTcO₄ versus HReO₄. Neither the oxygen charges in the bare MO₄⁻ nor those in the protonated HMO₄ account for the relative PAs. As remarked above, not only the O^δ...H bonds, but additionally the perturbations to all bonds in conversion of MO₄⁻ to HMO₄ need to be considered to effectively assess and predict PAs.

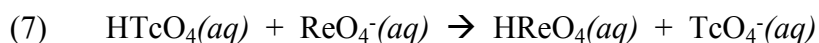
To the extent that relativistic effects influence the PAs of the MO₄⁻ species, the consequences should be greater for M = Re with nuclear charge Z=75, versus M = Tc with Z=43. Using the ADF code and the B3LYP hybrid functional yields non-relativistic PA[TcO₄⁻] = 307.77 kcal/mol and PA[ReO₄⁻] = 306.45 kcal/mol. These values are ca. 7 kcal/mol for Tc and 9 kcal/mol for Re higher than those obtained using Gaussian with the same functional and scalar relativistic ECPs. Applying a relativistic correction using ZORA with ADF yields PA[TcO₄⁻] = 306.75 kcal/mol and PA[ReO₄⁻] = 303.62 kcal/mol. The relativistic correction to the ADF ReO₄⁻ value, ΔPA = 2.83 kcal/mol, is indeed greater than that for TcO₄⁻, ΔPA = 1.02 kcal/mol. The ADF results suggest that without the reality of relativistic effects, the PAs of TcO₄⁻ and ReO₄⁻ would be even more similar. Notably, the PA ordering remains the same for the relativistic and non-relativistic ADF values, PA[TcO₄⁻] > PA[ReO₄⁻], and the difference between the relativistic ADF values, 3.13 kcal/mol, is close to the difference of 2.84 kcal/mol using Gaussian and ECPs.

Gould and Miller determined thermodynamics of rhenium species formed in flames.³⁵ Of particular relevance to the present study is the following studied reaction: e⁻ + HReO₄ → ReO₄⁻ + H. The enthalpy change for this reaction, 4±12 kcal/mol, combined with IE[H → H⁺ + e⁻] = 313.59 kcal/mol,³⁶ yields PA[ReO₄⁻] = 318±12 kcal/mol. All three PA[ReO₄⁻] values computed here,

particularly the relativistic ZORA value of 303.62 kcal/mol, are in reasonable accord with the experimental value.

Relationship between Gas and Solution Chemistry

As noted above, CID of $(\text{TcO}_4^-)(\text{H}^+)(\text{ReO}_4^-)$ essentially probes whether the enthalpy of proton transfer reaction (5), ΔH_5 , is positive or negative, to preferentially yield ReO_4^- or TcO_4^- , respectively. The experimental result that CID yields mostly ReO_4^- indicates that $\Delta H_5 > 0$. The B3LYP/SDD/6-31++G** computations properly provide a positive value for the enthalpy ΔH_5 , 2.85 kcal/mol, which is coincidentally identical to the free energy ΔG_5 computed at this level of theory (Table 2). The aqueous solution reaction corresponding to gas-phase reaction (5) is reaction (7). Proton association constants obtained for TcO_4^- and ReO_4^- in aqueous solution under identical conditions provide an equilibrium constant for reaction (7) of $K_7 = 0.49$ at 298 K,³⁷ which corresponds to $\Delta G_7 = 0.43$ kcal/mol.



The experimental result that the solution basicity of TcO_4^- is greater than that of ReO_4^- is in qualitative accord with the higher gas-phase PA of TcO_4^- versus ReO_4^- . However, even this qualitative accord is quite possibly fortuitous given the very different nature of gas-phase PA and solution basicity. Whereas gas-phase PA depends only on the binding energy to a proton, solution basicity reflects additionally the multifarious bonding transformations due to changes in solvation. In essence, the energy associated with the ensemble of ion-solution interactions cannot be simplified to consideration of only the anion-receptor interactions,³⁸ including when the “receptor” is a proton. Furthermore, whereas gas-phase PA probes the enthalpy of proton association, solution basicity reflects the free energy of association in which entropy effects are typically substantial.³⁸

Despite the need for discretion when inferring solution properties from those of constituent unsolvated gas-phase species, it is appealing—and reasonable—to cautiously employ simple molecular properties to rationalize, understand, and predict more complex condensed phase phenomena. The rather disparate charge distributions computed for TcO_4^- and ReO_4^- (Figure 6) are a case in point. The more energetically favorable hydration, and less effective extraction, of ReO_4^- versus TcO_4^- may reflect the generally greater “hydrophilicity” of ReO_4^- ,³¹ which can in turn be attributed to its more polar nature. It is additionally tempting to partly attribute the higher acidity of HReO_4 versus HTcO_4 to enhanced hydration of more polar ReO_4^- versus TcO_4^- , an effect that should preferentially favor dissociation of HReO_4 . However, this oversimplified assessment neglects differences between hydration of the undissociated acids. Specifically, the greater M-O^δ bond polarity in HReO_4 ($\delta = 0.57$) versus HTcO_4 ($\delta = 0.37$) should preferentially enhance hydration of HReO_4 , and thus suppress its dissociation and acidity relative to HTcO_4 . The result that computed molecular properties like atomic charges can be employed to rationalize contradictory effects illustrates the need for caution in inferring solution behavior from selected properties of isolated gas-phase species.

Conclusions

Gas-phase protonated dimer $(\text{TcO}_4^-)(\text{H}^+)(\text{ReO}_4^-)$ was produced by ESI in sufficient abundance for isolation and dissociation by CID. The dominant dissociation pathway to HTcO_4 and ReO_4^- reveals that $\text{PA}[\text{TcO}_4^-]$ is greater than $\text{PA}[\text{ReO}_4^-]$. Energies computed by DFT are in accord with this comparison, with the computed PAs differing by only $\sim 1\%$ (~ 3 kcal/mol) relative to their absolute values (~ 300 kcal/mol). Consideration of computed molecular properties indicates that the higher $\text{PA}[\text{TcO}_4^-]$ versus $\text{PA}[\text{ReO}_4^-]$ cannot be rationalized from differences in negative charges on the proton-receptor O atoms, which are more negative in the Re species. Instead, the entirety of bond formation and disruption needs to be considered to understand the results; the lower $\text{PA}[\text{ReO}_4^-]$ versus $\text{PA}[\text{TcO}_4^-]$ suggests greater disruption of more ionic Re-O bonds upon protonation. Although the relative PAs are in qualitative agreement with reports that TcO_4^- is a stronger aqueous base than ReO_4^- , restraint is advisable when inferring insights into complex condensed phase phenomena from simple gas-phase molecular properties.

Evaluating relative PAs of metal anion dimer complexes is a potential means to assess charge distributions and bonding in constituent bare and protonated species. It is anticipated that other such anions may present more substantial PA differences than do chemically very similar TcO_4^- and ReO_4^- . Generation by ESI of the dimer $(\text{TcO}_4^-)(\text{H}^+)(\text{ReO}_4^-)$ with a binding energy of only ~ 30 kcal/mol suggests that it should be feasible to prepare other such proton bound dimers. An extension of the present type of study would be CID of dimers containing actinide tetroxide anions like NpO_4^- and PuO_4^- .^{39,40} Dimer $(\text{NpO}_4^-)(\text{H}^+)(\text{PuO}_4^-)$ should have a simple proton-bridged structure, $[\text{O}_3\text{Np}-\text{O}\cdots\text{H}\cdots\text{OPuO}_3]^-$, CID of which would reveal the relative magnitudes of $\text{PA}[\text{NpO}_4^-]$ versus $\text{PA}[\text{PuO}_4^-]$. These relative PAs should reflect bonding differences between Np-O and Pu-O bonds, and their perturbations upon protonation.

Supporting Information

Complete citations for references 18 and 19; bond distances, NBO bond orders, and NPA charges of species in reactions (1) and (2); frequencies for Tc-O and Re-O vibrational modes; PAs of TcO_4^- and ReO_4^- calculated with different functionals and basis sets; CID mass spectra of $[(\text{L})(\text{H}^+)]$ and $(\text{TcO}_4^-)(\text{H}^+)(\text{ReO}_4^-)$; ESI mass spectrum of a $\text{L}/\text{TcO}_4^-/\text{ReO}_4^-$ solution; structures and energies of $(\text{L})[(\text{TcO}_4^-)(\text{H}^+)(\text{ReO}_4^-)]$.

Acknowledgements

This work was supported primarily by the Center for Actinide Science and Technology, an Energy Frontier Research Center funded by the U.S. Department of Energy, Office of Science, Basic Energy Sciences (DOE BES) under Award Number DE-SC0016568. WWL was supported by the DOE BES Heavy Element Chemistry Program at Lawrence Berkeley National Laboratory under Contract DE-AC02-05CH11231.

Table 1. Computed energies for different dissociations of (L)[(TcO₄⁻)(H⁺)(ReO₄⁻)] at the DFT/B3LYP/SDD/6-31G* level of theory (kcal/mol, zero point energy included).

| Dissociation Products | Energy |
|---|--------------------------|
| (L)(TcO ₄ ⁻) + HReO ₄ | ΔE = 17.23 |
| | ΔH = 16.89 |
| | ΔG = 7.44 |
| (L)(ReO ₄ ⁻) + HTcO ₄ | ΔE = 14.42 |
| | ΔH = 14.08 |
| | ΔG = 4.86 |
| (TcO ₄ ⁻)(H ⁺)(ReO ₄ ⁻) + L | ΔE = -16.84 ^a |
| | ΔH = -17.18 |
| | ΔG = -30.14 |

^aUsing the 6-311+G* basis set, the computed ΔE is -0.17 kcal/mol.

Table 2. Computed energies for dissociation of [(TcO₄⁻)(H⁺)(ReO₄⁻)]^a.

| Reaction ^b | Energy | SDD/ 6-31G* ^c | SDD/ 6-311+G* ^c | SDD/ 6-31++G** ^c | ZORA- B3LYP ^d | ZORA- B3LYP-D3 ^d |
|------------------------------|--------|-----------------------------|-------------------------------|--------------------------------|-----------------------------|--------------------------------|
| (1) | ΔE | 28.71 | 27.40 | 28.07 | 24.99 | 25.82 |
| | ΔH | 28.35 | 27.05 | 27.81 | 24.93 | 25.91 |
| | ΔG | 21.24 | 21.91 | 19.85 | 15.96 | 16.56 |
| (2) | ΔE | 31.84 | 29.99 | 30.92 | 28.12 | 28.95 |
| | ΔH | 31.47 | 29.66 | 30.66 | 28.07 | 29.05 |
| | ΔG | 25.04 | 25.13 | 22.70 | 19.09 | 19.69 |
| ΔH ₅ ^e | ΔE | 3.13 | 2.59 | 2.85 | 3.13 | 3.13 |
| | ΔH | 3.12 | 2.61 | 2.85 | 3.14 | 3.14 |
| | ΔG | 3.80 | 3.22 | 2.85 | 3.13 | 3.13 |

^aEnergies in kcal/mol at 298.15 K. Zero point energy is included.

^bReaction (1) products are HTcO₄ + ReO₄⁻; reaction (2) products are HReO₄ + TcO₄⁻.

^cUsing Gaussian09 DFT/B3LYP with the indicated basis set and ECP.

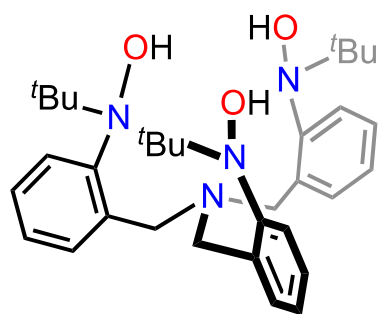
^dUsing the ADF code (scalar ZORA) with the indicated functional and ZORA-TZP basis sets.

^eDifference between the energies for (2) and (1).

Table 3. Selected bond distances (Å), NBO bond orders, and stretching frequencies (cm⁻¹) at the B3LYP/SDD/6-31++G* level of theory.

| | | TcO ₄ ⁻ | HTcO ₄ | ReO ₄ ⁻ | HReO ₄ | (TcO ₄ ⁻)(H ⁺)(ReO ₄ ⁻) ^a |
|------|------------------|-------------------------------|-------------------|-------------------------------|-------------------|--|
| M-O | <i>distance</i> | 1.733 | 1.696 | 1.754 | 1.719 | 1.708 / 1.738 |
| | <i>NBO</i> | 1.60 | 1.79 | 1.58 | 1.77 | 1.71 / 1.66 |
| | <i>frequency</i> | 915 | 986 | 943 | 965 | 976 / 967 |
| M-OH | <i>distance</i> | - | 1.882 | - | 1.891 | 1.806 / 1.796 |
| | <i>NBO</i> | - | 0.91 | - | 0.91 | 1.16 / 1.27 |
| | <i>frequency</i> | - | 692 | - | 684 | 881 / 743 |
| MO-H | <i>distance</i> | - | 0.971 | - | 0.970 | 1.117 / 1.291 |
| | <i>NBO</i> | - | 0.71 | - | 0.70 | 0.43 / 0.27 |

^a Parameters are expressed as "M = Tc / M = Re".



H₃TriNOx (L)
C₃₃H₄₈O₃N₄ / 548 Da

Figure 1. Schematic structure of the H₃TriNOx ligand (L).

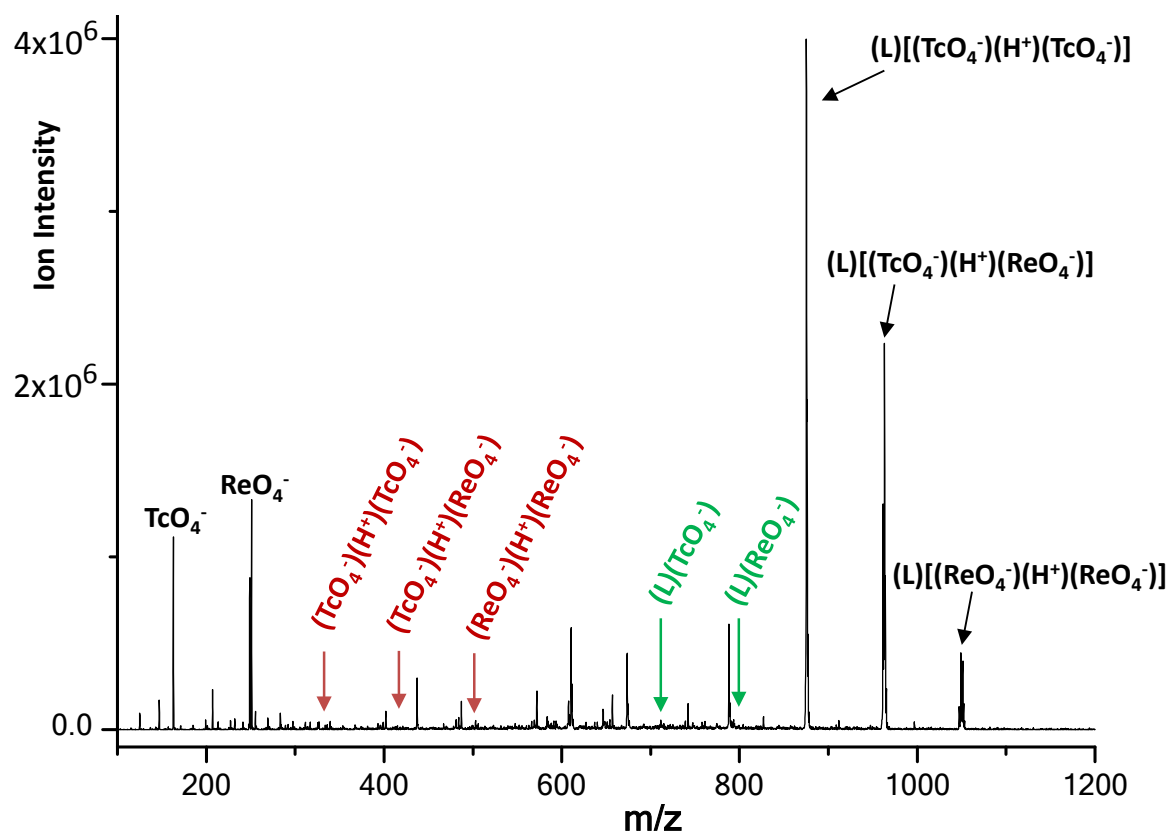


Figure 2. ESI mass spectrum of solution of H₃TriNOx (L), NH₄TcO₄ and NH₄ReO₄ (concentration ratio 1:5:5). The *m/z* values of selected minor or minuscule products are as indicated by arrows and compositions in red (dimers) and green (monomers). Unassigned peaks may be due to ligand fragmentation as shown in SI Figure S1. Spectra with *y*-axis magnification to better reveal labelled low-intensity peaks are in SI Figure S2.

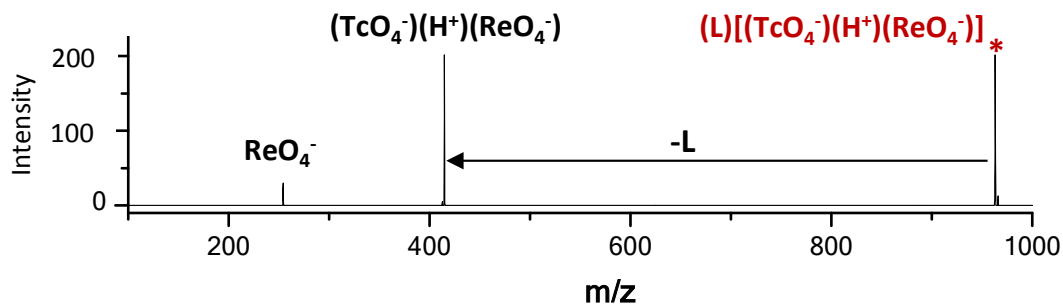


Figure 3. CID mass spectrum of $(L)[(TcO_4^-)(H^+)(ReO_4^-)]$ where $L = H_3TriNOx$. The nominal CID voltage was 0.20 V. The dominant CID pathway is loss of ligand L.

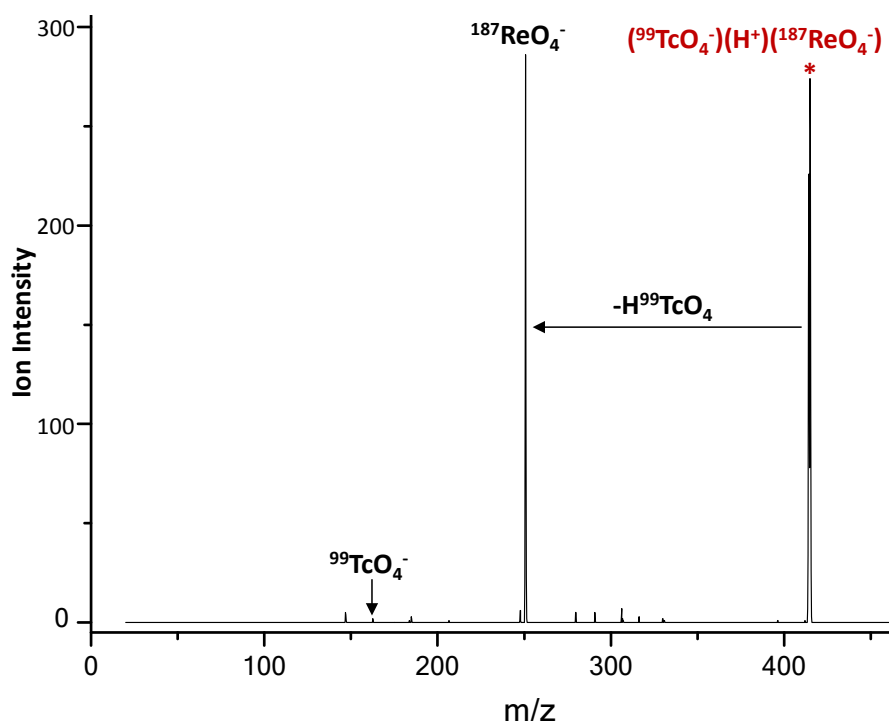


Figure 4. CID mass spectrum of $(TcO_4^-)(H^+)(ReO_4^-)$ at a nominal CID voltage of 0.25 V. The dominant CID anion product is ReO_4^- via reaction (1). The minor ($<1\%$) yield of TcO_4^- is indicated.

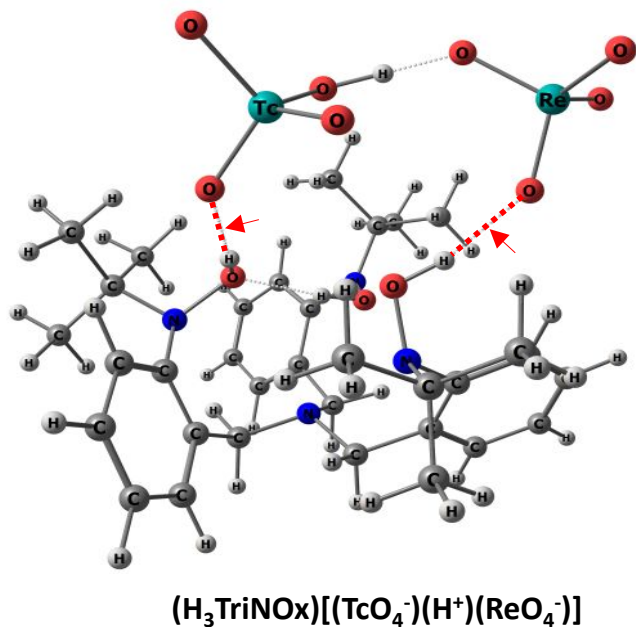


Figure 5. Structure of $[(H_3TriNOx)(TcO_4^-)(H^+)(ReO_4^-)]$ computed at the B3LYP/SDD/6-31G* level of theory. The two hydrogen bonds between metal oxo and ligand hydroxyl groups are indicated.

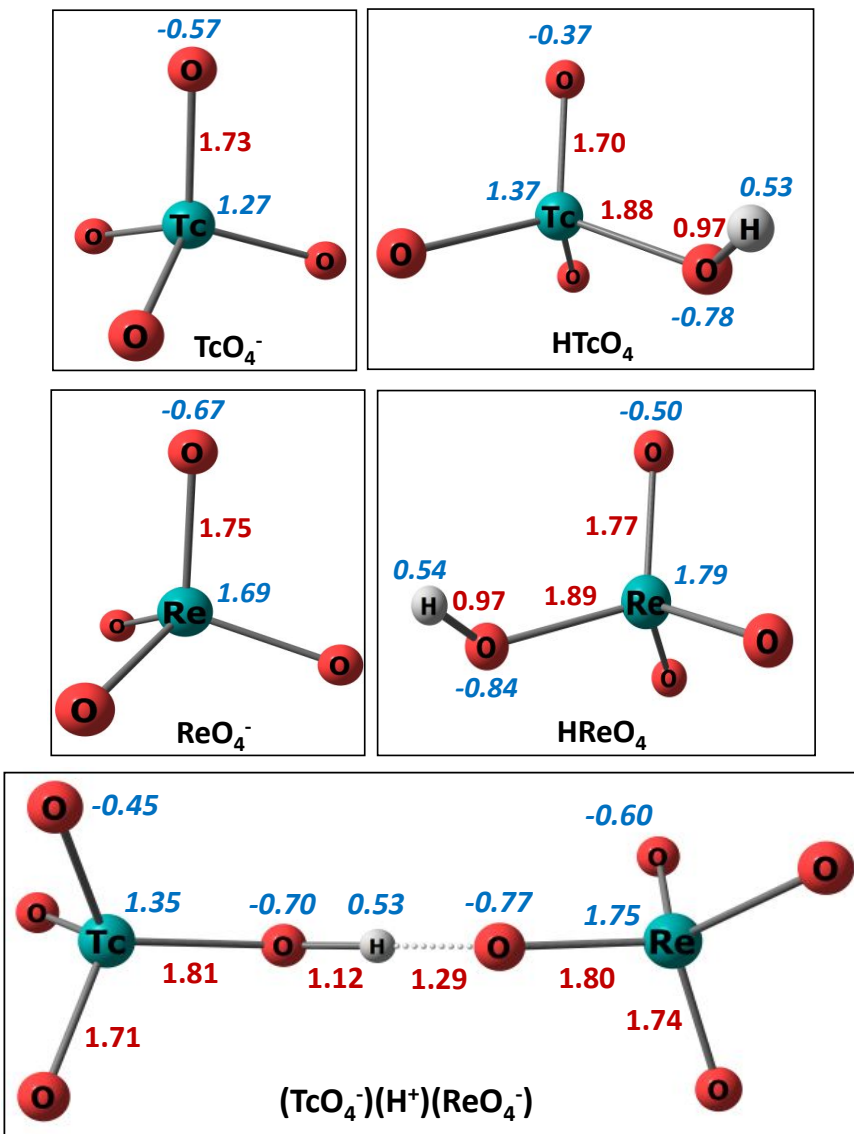


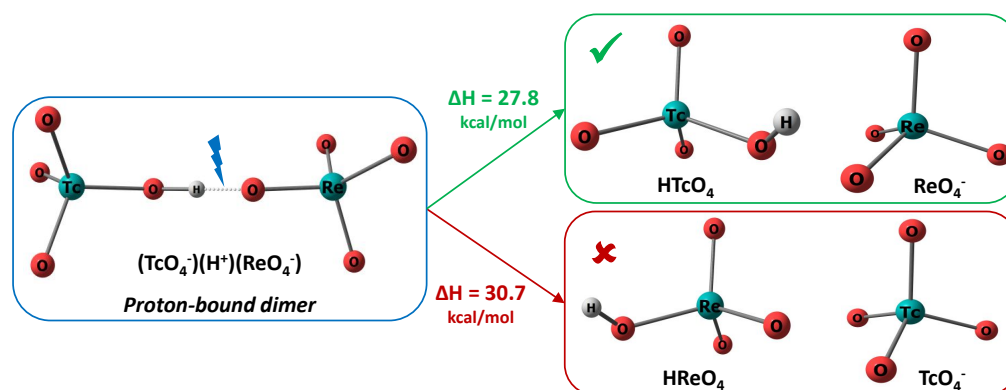
Figure 6. Structures of the species in reactions (1) and (2) optimized at the B3LYP/SDD/6-31++G** level of theory. Selected bond distances (Å) are in red; NPA atomic charges are in blue italics.

References

- (1) Choppin, G. R. Inner versus outer sphere complexation of f-elements. *J Alloy Compd* **1997**, *249*, 9-13.
- (2) Williams, C. D.; Carbone, P. A classical force field for tetrahedral oxyanions developed using hydration properties: The examples of pertechnetate (TcO₄⁻) and sulfate (SO₄²⁻). *J Chem Phys* **2015**, *143*.
- (3) Chen, F. R.; Burns, P. C.; Ewing, R. C. Near-field behavior of Tc-99 during the oxidative alteration of spent nuclear fuel. *J Nucl Mater* **2000**, *278*, 225-232.
- (4) Dadachova, E.; Bouzhzah, B.; Zuckier, L. S.; Pestell, R. G. Rhenium-188 as an alternative to iodine-131 for treatment of breast tumors expressing the sodium/iodide symporter (NIS). *Nucl Med Biol* **2002**, *29*, 13-18.
- (5) Zhang, D. W.; Ronson, T. K.; Mosquera, J.; Martinez, A.; Nitschke, J. R. Selective Anion Extraction and Recovery Using a (Fe₄L₄)-L-II Cage. *Angew Chem Int Edit* **2018**, *57*, 3717-3721.
- (6) Ravi, A.; Oshchepkov, A. S.; German, K. E.; Kirakosyan, G. A.; Safonov, A. V.; Khrustalev, V. N.; Kataev, E. A. Finding a receptor design for selective recognition of perrhenate and pertechnetate: hydrogen vs. halogen bonding. *Chem Commun* **2018**, *54*, 4826-4829.
- (7) Alberto, R.; Bergamaschi, G.; Braband, H.; Fox, T.; Amendola, V. (TcO₄⁻)-Tc-99-: Selective Recognition and Trapping in Aqueous Solution. *Angew Chem Int Edit* **2012**, *51*, 9772-9776.
- (8) Mei, L.; Li, F. Z.; Lan, J. H.; Wang, C. Z.; Xu, C.; Deng, H.; Wu, Q. Y.; Hu, K. Q.; Wang, L.; Chai, Z. F.; Chen, J.; Gibson, J. K.; Shi, W. Q. Anion-adaptive crystalline cationic material for (TcO₄⁻)-Tc-99 trapping. *Nat Commun* **2019**, *10*.
- (9) Bogart, J. A.; Lippincott, C. A.; Carroll, P. J.; Schelter, E. J. An Operationally Simple Method for Separating the Rare-Earth Elements Neodymium and Dysprosium. *Angew Chem Int Edit* **2015**, *54*, 8222-8225.
- (10) Cheisson, T.; Jian, J. W.; Su, J.; Eaton, T. M.; Gau, M. R.; Carroll, P. J.; Batista, E. R.; Yang, P.; Gibson, J. K.; Schelter, E. J. Halide anion discrimination by a tripodal hydroxylamine ligand in gas and condensed phases. *Phys Chem Chem Phys* **2019**, *21*, 19868-19878.
- (11) Dobbins, J. T.; Colehour, J. K. The preparation of perrhenic acid. *J Am Chem Soc* **1934**, *56*, 2054-2054.
- (12) Cobble, J. W.; Smith, W. T.; Boyd, G. E. Thermodynamic Properties of Technetium and Thenuim Compounds .2. Heats of Formation of Technetium Heptoxide and Pertechnic Acid, Potential of the Technetium(Iv)-Technetium(Vii) Couple, and a Potential Diagram for Technetium. *J Am Chem Soc* **1953**, *75*, 5777-5782.
- (13) Rulfs, C. L.; Pacer, R. A.; Hirsch, R. F. Pertechnic Acid - an Aperiodic Variation in Acid Strength. *Nature* **1963**, *199*, 66-&.
- (14) Mcluckey, S. A.; Cameron, D.; Cooks, R. G. Proton Affinities from Dissociations of Proton-Bound Dimers. *J Am Chem Soc* **1981**, *103*, 1313-1317.
- (15) Armentrout, P. B. Special feature: Commentary - Is the kinetic method a thermodynamic method? *J Mass Spectrom* **1999**, *34*, 74-78.
- (16) Cooks, R. G.; Patrick, J. S.; Kotiaho, T.; Mcluckey, S. A. Thermochemical Determinations by the Kinetic Method. *Mass Spectrom Rev* **1994**, *13*, 287-339.
- (17) Hou, G. L.; Wang, X. B.; Valiev, M. Formation of (HCOO⁻)(H₂SO₄) Anion Clusters: Violation of Gas-Phase Acidity Predictions. *J Am Chem Soc* **2017**, *139*, 11321-11324.
- (18) Rios, D.; Rutkowski, P. X.; Shuh, D. K.; Bray, T. H.; Gibson, J. K.; Van Stipdonk, M. J. Electron transfer dissociation of dipositive uranyl and plutonyl coordination complexes. *J Mass Spectrom* **2011**, *46*, 1247-1254.
- (19) Frish, M.; etal.: Gaussian 09 Revision C.01. 2010.

- (20) Baerends, E.; et al.: ADF 2017, SCM. Vrije Universiteit: Amsterdam, 2017.
- (21) te Velde, G.; Bickelhaupt, F. M.; Baerends, E. J.; Guerra, C. F.; Van Gisbergen, S. J. A.; Snijders, J. G.; Ziegler, T. Chemistry with ADF. *J Comput Chem* **2001**, *22*, 931-967.
- (22) Cao, X. Y.; Dolg, M.; Stoll, H. Valence basis sets for relativistic energy-consistent small-core actinide pseudopotentials. *J Chem Phys* **2003**, *118*, 487-496.
- (23) Krishnan, R.; Binkley, J. S.; Seeger, R.; Pople, J. A. Self-Consistent Molecular-Orbital Methods .20. Basis Set for Correlated Wave-Functions. *J Chem Phys* **1980**, *72*, 650-654.
- (24) Becke, A. D. Density-Functional Thermochemistry .3. The Role of Exact Exchange. *J Chem Phys* **1993**, *98*, 5648-5652.
- (25) Lee, C. T.; Yang, W. T.; Parr, R. G. Development of the Colle-Salvetti Correlation-Energy Formula into a Functional of the Electron-Density. *Phys Rev B* **1988**, *37*, 785-789.
- (26) Reed, A. E.; Curtiss, L. A.; Weinhold, F. Intermolecular Interactions from a Natural Bond Orbital, Donor-Acceptor Viewpoint. *Chem Rev* **1988**, *88*, 899-926.
- (27) Glendening, E. D.; Badenhoop, J. K.; Reed, A. E.; Carpenter, J. E.; Bohmann, J. A.; Morales, C. M.; Weinhold, F.: NBO 6.0. University of Wisconsin: Madison, WI, 2017.
- (28) Grimme, S.; Antony, J.; Ehrlich, S.; Krieg, H. A consistent and accurate ab initio parametrization of density functional dispersion correction (DFT-D) for the 94 elements H-Pu. *J Chem Phys* **2010**, *132*.
- (29) Van Lenthe, E.; Baerends, E. J.; Snijders, J. G. Relativistic Regular 2-Component Hamiltonians. *J Chem Phys* **1993**, *99*, 4597-4610.
- (30) Van Lenthe, E.; Baerends, E. J. Optimized slater-type basis sets for the elements 1-118. *J Comput Chem* **2003**, *24*, 1142-1156.
- (31) Katayev, E. A.; Boev, N. V.; Khrustalev, V. N.; Ustynyuk, Y. A.; Tananaev, I. G.; Sessler, J. L. Bipyrrrole- and dipyrromethane-based amido-imine hybrid macrocycles. New receptors for oxoanions. *J Org Chem* **2007**, *72*, 2886-2896.
- (32) Chen, W. J.; Zhai, H. J.; Huang, X.; Wang, L. S. On the electronic structure of mono-rhenium oxide clusters: ReO_n⁻ and ReO_n (n=3, 4). *Chem Phys Lett* **2011**, *512*, 49-53.
- (33) Bridgeman, A. J.; Cavigliasso, G. Density-functional investigation of bonding in tetrahedral MO₄ anions. *Polyhedron* **2001**, *20*, 2269-2277.
- (34) Schwerdtfeger, P.; Nagle, K. J. Table of Static Dipole Polarizabilities of the Neutral Elements in the Periodic Table (vol 117, pg 1200, 2018). *Mol Phys* **2019**, *117*, 1585-1585.
- (35) Gould, R. K.; Miller, W. J. Electron Attachment and Compound Formation in Flames .6. Negative-Ion and Compound Formation in Flames Containing Rhenium and Potassium. *J Chem Phys* **1975**, *62*, 644-649.
- (36) Lias, S. G.; Rosenstock, H. M.; Draxl, K.; Steiner, B. W.; Herron, J. T.; Jolmes, J. L.; Levin, R. D.; Liebman, J. F.; Kafafi, S. A.: NIST Chemistry WebBook. NIST Standard Reference Database Number 69.; National Institute of Standards and Technology: Gaithersburg, MD, 2018.
- (37) Nakashima, T.; Lieser, K. H. Proton Association of Pertechnetate, Perrhenate and Perchlorate Anions. *Radiochim Acta* **1985**, *38*, 203-206.
- (38) Schmidtchen, F. P. Hosting anions. The energetic perspective. *Chem Soc Rev* **2010**, *39*, 3916-3935.
- (39) Gibson, J. K.; de Jong, W. A.; Dau, P. D.; Gong, Y. Heptavalent Actinide Tetroxides NpO₄⁻ and PuO₄⁻: Oxidation of Pu(V) to Pu(VII) by Adding an Electron to PuO₄. *J Phys Chem A* **2017**, *121*, 9156-9162.
- (40) Wren, J. E. C.; Schreckenbach, G. Neptunium(VII) in high-ionic-strength alkaline solutions - [NpO₂(OH)(4)](1-) or [NpO₄(OH)(2)](3-)? *Can J Chem* **2009**, *87*, 1436-1443.

Table of Contents



Endeavoring to understand the basis for the difference between proton affinities of pertechnetate and perrhenate anions reveals complexity in a seemingly straightforward phenomenon.